# Factors Affecting the Energy-Dispersive X-Ray Fluorescence (EDXRF) Analysis of Archaeological Obsidian

**Chapter** · January 2011

DOI: 10.1007/978-1-4419-6886-9_3



**5 authors**, including:

Michael Steven Shackley
University of California, Berk…

**79** PUBLICATIONS **1,177**
CITATIONS

SEE PROFILE

# Chapter 3
# Factors Affecting the Energy-Dispersive X-Ray Fluorescence (EDXRF) Analysis of Archaeological Obsidian

**M. Kathleen Davis, Thomas L. Jackson, M. Steven Shackley, Timothy Teague, and Joachim H. Hampel**

## Introduction to the Springer Reprint

At the 28th International Symposium on Archaeometry in 1992 in Los Angeles, Joachim Hampel, Tom Jackson, and Steve Shackley, presented two poster presentations on size and surface effects in the energy-dispersive X-ray fluorescence (EDXRF) analysis of archaeological obsidian (Jackson and Hampel, 1992; Shackley and Hampel, 1992). Joachim Hampel, who was the XRF technician in what was then called the Department of Geology and Geophysics, and is now Earth and Planetary Sciences at Berkeley, was instrumental in worrying about these issues and was just as instrumental in shaping the authors of this 1998 paper, as well as many others from the 1970s through the 1990s till his retirement. In 1984, in Richard Hughes (1984) volume on Great Basin obsidian, his "Technical considerations in X-ray fluorescence analysis of obsidian" was the first major step toward understanding the real resolution of EDXRF for archaeological obsidian. Kathy Davis, the primary author and experimental genius who did the work and synthesis for this chapter, provided one of the most referenced papers on the subject in archaeology today. Indeed, the size and surface effects that are integrated into "normal" science in EDXRF studies are based on this project and paper. The Lundblad et al. paper presented here is very much based on the assumptions generated by this paper and replicated in basalt studies, as discussed by these authors. For this reason, we republish this important work more than 10 years later, but it is just as critical today. I have eliminated the discussion of EDXRF theory and instrumentation, including two figures, and refer the reader to Chap. 2, which is a much more intensive exploration of the subject with the archaeologist in mind. Minor editorial changes have been made to fit the publisher's guidelines. Otherwise, the text, tables, and illustrations are exactly as in the original.

M. Steven Shackley (✉)
Far Western Anthropological Research Group, 2727 Del Rio Place, Suite A, Davis, CA 95618, USA
e-mail: shackley@berkeley.edu

M.S. Shackley (ed.), *X-Ray Fluorescence Spectrometry (XRF) in Geoarchaeology*,
DOI 10.1007/978-1-4419-6886-9_3, 

## Introduction

Non-destructive X-ray fluorescence (XRF) is now widely accepted by archaeologists as a tool for the identification of the geologic origins of obsidian artifact raw material, and to a lesser extent, artifacts of basalt and other volcanic rock. While the advantages of the non-destructive EDXRF approach are obvious for artifact studies, analysis of unmodified obsidian rather than powdered samples contributes to an already long list of analytical uncertainties inherent in XRF analysis. Understanding the magnitude and source of these uncertainties is crucial to accurate ascription of artifacts to source, particularly when characterizing artifacts from closely related sources. Previous attempts to quantify analytical uncertainties in non-destructive analysis have focused on errors related to variation in artifact size and surface morphology (Bouey, 1991; Jackson and Hampel, 1992; Shackley and Hampel, 1992; Davis, 1994). These studies suggest that artifact size is potentially the more important contributor although the actual magnitude of errors due to surface morphology remains poorly understood.

Elaborating on these earlier studies, this chapter attempts to quantify errors associated with artifact size and surface morphology via two different experiments. The first experiment is an analysis of unmodified samples of various sizes made from a single obsidian core; the second involves multiple analyses of flaked and powdered samples to measure errors related to artifact surface variability. All samples are analyzed for the elements Ti, Mn, Fe, Zn, Pb, Rb, Sr, Y, Zr, and Ba, using analyte/scatter and peak ratio techniques to compensate for errors associated with the analysis of unmodified obsidian. Since both experiments involve multiple analyses of samples and comparisons to powdered samples, it is also hoped that the data may be useful as a general indicator of the accuracy and precision of the method.

## Methods

### *Size Experiment*

To determine the limits of the scatter and peak ratio techniques as discussed in Chap. 2 and to correct for artifact size, we analyzed 20 samples of varying thickness and diameter prepared from a single core of obsidian from the Glass Mountain source in northeastern California. Samples were prepared at the Department of Geology and Geophysics, University of California at Berkeley, and are also the subject of a paper by Jackson and Hampel (1992). Samples were carefully cut and ground to specified dimensions using a lapidary saw and abrasive, and are smooth and polished on both target and opposite sides. The first eight samples are round, with a fixed diameter of 25 mm and thicknesses of 0.03, 0.2, 0.5, 1, 2, 3, 4, and 5 mm. By stacking various combinations of these eight samples, analyses were also conducted for sample thicknesses of 6–11 mm, and for the 1.2, 1.5, 1.7, and 2.5 mm thick samples reported in the mid-Z analysis (Table 3.2). The remaining 12 samples are square, measuring 3, 5, 10, or 15 mm on a side with thicknesses of 1, 2, and 3 mm for each.

**Table 3.1** Selected trace element concentrations of two international rock standards

| | Zn | Pb | Rb | Sr | Y | Zr | Ti | Mn | Fe | Ba | Ba (Am) |
|---|---|---|---|---|---|---|---|---|---|---|---|
| RGM-1 | | | | | | | | | | | |
| Govindaraju 1989 | 32 | 24 | 149 | 108 | 25 | 219 | 1601 | 279 | 1.86 | 807 | 807 |
| (this study) | 44 | 20 | 149 | 107 | 25 | 218 | 1673 | 288 | 2 | 794 | 785 |
| ± | 4.9 | 2.5 | 2.8 | 6.3 | 1.6 | 5.1 | 81.3 | 29.7 | 0.10 | 9.2 | 12.8 |
| NBS-278 | | | | | | | | | | | |
| Govindaraju 1989 | 55 | 16.4 | 127.5 | 63.5 | 41 | 295 | 1469 | 403 | 2.04 | 1140 | 1140 |
| (this study) | 53 | 16 | 128 | 65 | 40 | 284 | 1407 | 450 | 2 | – | – |
| ± | 5.1 | 2.4 | 2.7 | 6.3 | 1.6 | 5.2 | 81.3 | 29.8 | 0.10 | – | – |

Plus or minus values represent a combined estimate of counting and fitting error uncertainties. All values are in ppm with the exception of Fe ($Fe_2O_3^T$), which is in weight percent. RGM-1 is a U.S. Geological Survey rhyolite (obsidian) standard, and NBS-278 is a National Bureau of Standards obsidian standard. Values for barium acquired with the $^{241}Am$ radioisotope source are labeled Ba(Am)

## *Surface Variability Experiment*

A second experiment, using a different set of obsidian samples, was devised to measure errors resulting from the irregular surfaces of obsidian artifacts. These samples, also prepared at the Department of Geology and Geophysics at Berkeley, are the subject of a paper on surface effects by Shackley and Hampel (1992). With a fixed diameter of 25 mm, the target side of each sample has been flaked with a copper flaking tool to approximate the surface of a typical flaked stone artifact. Ten such samples are analyzed here, five from the Bodie Hills source located in eastern California and five from the Napa Valley source located in the North Coast Ranges of California. Each set of five samples, designated here BH-1 through BH-5 for Bodie Hills, and NV-1 through NV-5 for Napa Valley, was prepared from a single core of obsidian. The Bodie Hills samples range from 5 to 7 mm thick, while the Napa Valley samples range from 8 to 13 mm thick.

The flaked surface of each sample was analyzed in a random orientation and then rotated 45, 90, 180, 270, and 315° from the original orientation for five subsequent analyses. These results were then compared to analyses of pressed powder samples, one each of Bodie Hills and Napa Valley obsidian, which were acquired in the same six orientations. The Bodie Hills and Napa Valley powdered samples were not prepared from the same core as the flaked samples, and thus are not strictly comparable. However, our primary concern here is the comparison of relative and not absolute errors. Bodie Hills and Napa Valley powdered samples were chosen so that they would have peak counts comparable to those of the flaked samples. Two additional powdered samples, U.S. Geological Survey (USGS) standard RGM-1

**Table 3.2** Trace element values for unmodified (i.e., unpowdered) Glass Mountain obsidian of varying diameter and thickness

| Diameter (mm) | Thickness (mm) | Zn | Pb | Rb | Sr | Y | Zr | Fe/ Mn | Fe/ Ti | Ti | Mn | Fe | Ba | Ba(Am) |
|---|---|---|---|---|---|---|---|---|---|---|---|---|---|---|
| *Control group* | | | | | | | | | | | | | | |
| 25 | 11 | 38 | 20 | 152 | 112 | 29 | 233 | 67 | 35 | 1576 | 281 | 1.87 | 781 | 533 |
| 25 | 10 | 41 | 21 | 156 | 111 | 29 | 233 | 69 | 36 | 1560 | 270 | 1.87 | 813 | 538 |
| 25 | 9 | 38 | 25 | 155 | 112 | 28 | 234 | 63 | 34 | 1620 | 297 | 1.87 | 794 | 539 |
| 25 | 8 | 38 | 21 | 155 | 115 | 28 | 236 | 67 | 35 | 1605 | 279 | 1.87 | 824 | 553 |
| 25 | 7 | 43 | 23 | 161 | 112 | 25 | 229 | 68 | 34 | 1630 | 274 | 1.88 | 778 | 559 |
| 25 | 6 | 39 | 24 | 154 | 111 | 27 | 235 | 65 | 36 | 1545 | 286 | 1.86 | 798 | 564 |
| 25 | 5 | 34 | 20 | 158 | 112 | 27 | 230 | 71 | 35 | 1635 | 268 | 1.91 | 767 | 597 |
| 25 | 4 | 35 | 24 | 154 | 114 | 27 | 231 | 75 | 35 | 1613 | 256 | 1.93 | 814 | 640 |
| | Mean | 38 | 22 | 156 | 112 | 28 | 233 | 68 | 35 | 1598 | 276 | 1.9 | 796 | 565 |
| | SD | 2.8 | 1.9 | 2.6 | 1.5 | 1.2 | 2.5 | 3.7 | 0.6 | 33.4 | 12.3 | 0.03 | 20.2 | 36.4 |
| | CV | 7.4 | 8.6 | 1.7 | 1.4 | 4.4 | 1.1 | 5.5 | 1.8 | 2.1 | 4.5 | 1.4 | 2.5 | 6.4 |
| *Fixed diameter* | | | | | | | | | | | | | | |
| 25 | 3 | **47** | 23 | 158 | 115 | 27 | 232 | 73 | 34 | 1633 | 256 | 1.90 | 793 | 642 |
| 25 | 2.5 | 36 | **15** | 154 | 115 | 25 | 235 | | | | | | | |
| 25 | 2 | 44 | 22 | 157 | **117** | 30 | 234 | 75 | 34 | 1624 | **247** | 1.87 | 815 | **670** |
| 25 | 1.7 | **45** | 20 | **161** | **116** | 26 | 230 | | | | | | | |
| 25 | 1.5 | **55** | 21 | 161 | **119** | 27 | 235 | | | | | | | |
| 25 | 1.2 | **50** | 19 | **172** | **123** | **31** | 238 | | | | | | | |
| 25 | 1 | **47** | 24 | **184** | **130** | 28 | **250** | 74 | 35 | 1597 | 252 | 1.87 | 784 | **730** |
| 25 | 0.5 | **61** | **32** | **207** | **145** | 29 | **270** | 71 | 34 | 1638 | 260 | 1.87 | 755 | **744** |
| 25 | 0.2 | **86** | **45** | **251** | **167** | **35** | **285** | 74 | 34 | 1630 | 254 | 1.89 | 784 | **770** |
| 25 | 0.03 | **185** | **60** | **240** | **159** | 29 | **256** | 65 | **30** | **1416** | **223** | **1.43** | **602** | **1177** |
| *Fixed thickness* | | | | | | | | | | | | | | |
| 25 | 3 | **47** | 23 | 158 | 115 | 27 | 232 | 73 | 34 | 1633 | 256 | 1.90 | 793 | 642 |
| 15 | 3 | 36 | 20 | 155 | 115 | 27 | 234 | 75 | 36 | 1536 | **245** | 1.84 | **852** | 592 |
| 10 | 3 | **59** | 22 | 151 | 110 | **25** | 231 | 71 | 36 | **994** | **164** | **1.14** | 824 | **476** |
| 5 | 3 | **56** | 18 | **135** | **98** | 27 | **205** | 71 | 35 | **275** | **38** | **0.18** | **656** | **221** |
| 3 | 3 | **45** | **11** | **102** | **88** | **20** | **180** | **55** | 35 | **130** | **18** | **0.00** | **418** | **93** |
| 25 | 2 | 44 | 22 | 157 | **117** | 30 | 234 | 75 | 34 | 1624 | **247** | 1.87 | 815 | **670** |
| 15 | 2 | **51** | 19 | 151 | 114 | **31** | 228 | 76 | 36 | 1604 | 254 | 1.93 | **845** | **659** |
| 10 | 2 | 42 | 20 | 161 | 115 | 27 | **239** | 74 | 34 | **987** | **150** | **1.08** | 780 | **417** |
| 5 | 2 | **69** | **15** | **135** | **95** | **22** | **201** | **59** | **28** | **339** | **48** | **0.20** | **644** | **158** |
| 3 | 2 | **49** | **16** | **108** | **74** | **17** | **162** | **91** | 34 | **139** | **12** | **0.01** | **410** | **64** |
| 25 | 1 | **47** | 24 | **184** | **130** | 28 | **250** | 74 | 35 | 1597 | 252 | 1.87 | 784 | **730** |
| 15 | 1 | 37 | 26 | **178** | **128** | 26 | **248** | 70 | 35 | **1399** | **235** | **1.65** | 769 | **477** |
| 10 | 1 | **47** | **17** | **175** | **124** | 27 | **245** | 71 | 34 | **953** | **152** | **1.04** | 805 | **360** |
| 5 | 1 | **65** | 26 | **133** | **91** | **21** | **194** | 75 | **29** | **332** | **38** | **0.20** | **568** | **111** |
| 3 | 1 | 41 | **14** | **100** | **76** | **24** | **160** | **97** | 34 | **131** | **10** | **-0.00** | **274** | **34** |

All element values are expressed in ppm, with the exception of Fe/Mn and Fe/Ti peak ratios, and Fe ($Fe_2O_3^T$), which is expressed in weight percent. Values for barium acquired with the $^{241}Am$ radioisotope source are labeled Ba(Am). Values in the lower half of the table appear in bold type when they differ significantly (two sample *t*-test with $\alpha = 0.05$) from the control group above

and Geological Survey of Japan standard JR-2, were also included in the analysis and analyzed in the six orientations described above.

## *Analytical Conditions*

Both sample sets analyzed in this study were subjected to the following four procedures. Analyses for the elements Ti, Mn, Fe, Zn, Pb, Rb, Sr, Y, Zr, and Ba were conducted on a Spectrace 5000 EDXRF spectrometer, at BioSystems Analysis Inc. The Spectrace 5000 is equipped with a Si(Li) detector with a resolution of 155 eV FWHM for 5.9 keV X-rays (at 1,000 counts per second) in an area 30 $mm^2$. Signals from the spectrometer are amplified and filtered by a time variant pulse processor and sent to a 100 MHz Wilkinson type analog-to-digital converter. The X-ray tube employed is a bremsstrahlung type, with an Rh target and a 5 mil Be window. The tube is driven by 50 kV, 1 mA high voltage power supply, providing a voltage range of 4–50 kV (Fig. 3.1a)

For analysis of the mid-Z elements (Zn, Pb, Rb, Sr, Y, and Zr), the Rh X-ray tube is operated at 30 kV, 0.30 mA (pulsed), with a 0.127 mm Pd filter. Analytical lines used are Zn (K-a), Pb (L-a), Rb (K-a), Sr (K-a), Y (K-a), and Zr (K-a). Samples are scanned for 200 s live-time in an air path. Peak intensities for the above elements are calculated as ratios to the Compton scatter peak of rhodium and converted to parts-per-million (ppm) by weight using linear regressions derived from the analysis of 20 USGS, U.S. National Bureau of Standards (NBS) and Geological Survey

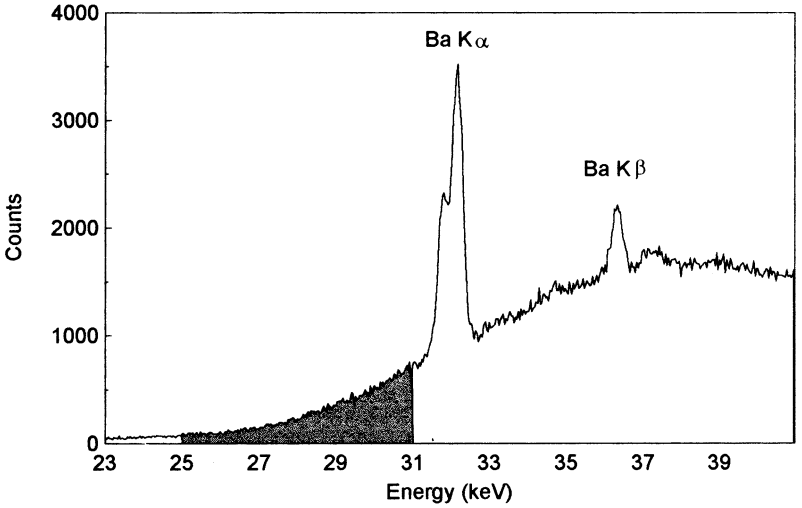


**Fig. 3.1** X-ray spectrum of a sample of unmodified Glass Mountain obsidian acquired at 50 kV showing the K-a and K-b peaks of Ba. The darkened bremsstrahlung region between 25 and 31 keV is used to correct for sample mass and thickness

of Japan (GSJ) rock standards. The analyte/Compton scatter ratio is employed to correct for variation in sample size, surface morphology, and sample matrix (see Chap. 2) (Fig. 3.2).

For analysis of the elements Ti ($TiO_2$), Mn (MnO), and Fe ($Fe_2O_3^T$), the X-ray tube is operated at 12 kV, 0.27 mA with a 0.127 mm aluminum filter. Samples are scanned for 200 s live-time in a vacuum path. Element values are reported in two ways: in units of concentration (parts per million for Ti and Mn, and weight percent for total Fe); and as Fe/Mn and Fe/Ti peak ratios. Peak ratios are calculated as simple ratios of extracted peak intensities (Kα and Kβ). Concentration values are calculated using linear regressions derived from the analysis of 13 standards from the USGS, the NBS and the GSJ. These values are reported to better evaluate the precision of each measurement. It should be noted that the concentration values are *not* corrected against a spectral reference, however, and are corrected for matrix effects only to the extent that the concentration range of Fe is limited in the chosen standards. As a result, large errors are evident among the smaller samples (Fig. 3.3).

For analysis of Ba, the X-ray tube is operated at 50 kV, 0.25 mA with a 0.63 mm Cu filter in the X-ray path. Samples are scanned for 200 s live-time in an air path. Trace element intensities for Ba, extracted from a net fit of the Kα peak, are calculated as ratios to the Bremsstrahlung region between 25.0 and 30.98 keV (Fig. 3.1b). Ppm values are generated using a polynomial regression derived from the analysis of eight USGS and eight GSJ rock standards.

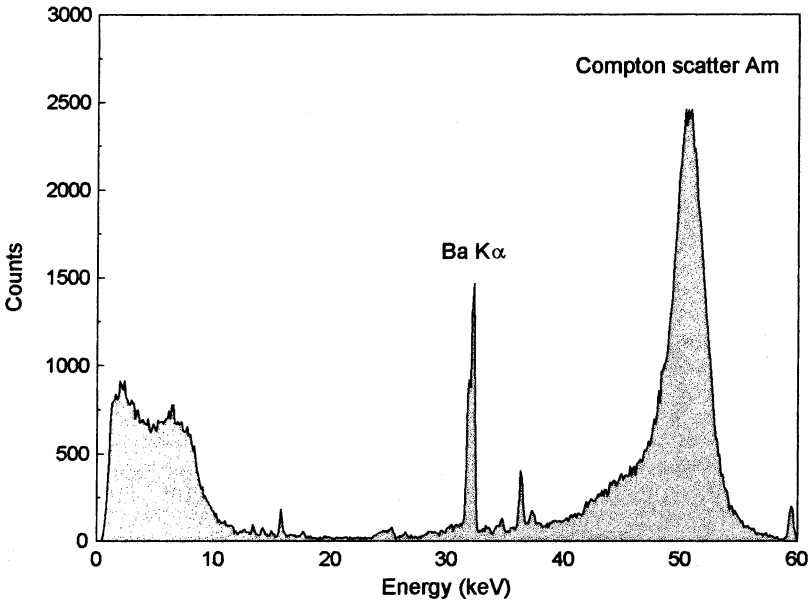


**Fig. 3.2** X-ray spectrum of unmodified Glass Mountain obsidian acquired using an $^{241}Am$ radioisotope source. Labeled are the K-a peak of Ba and the Compton scatter peak Am

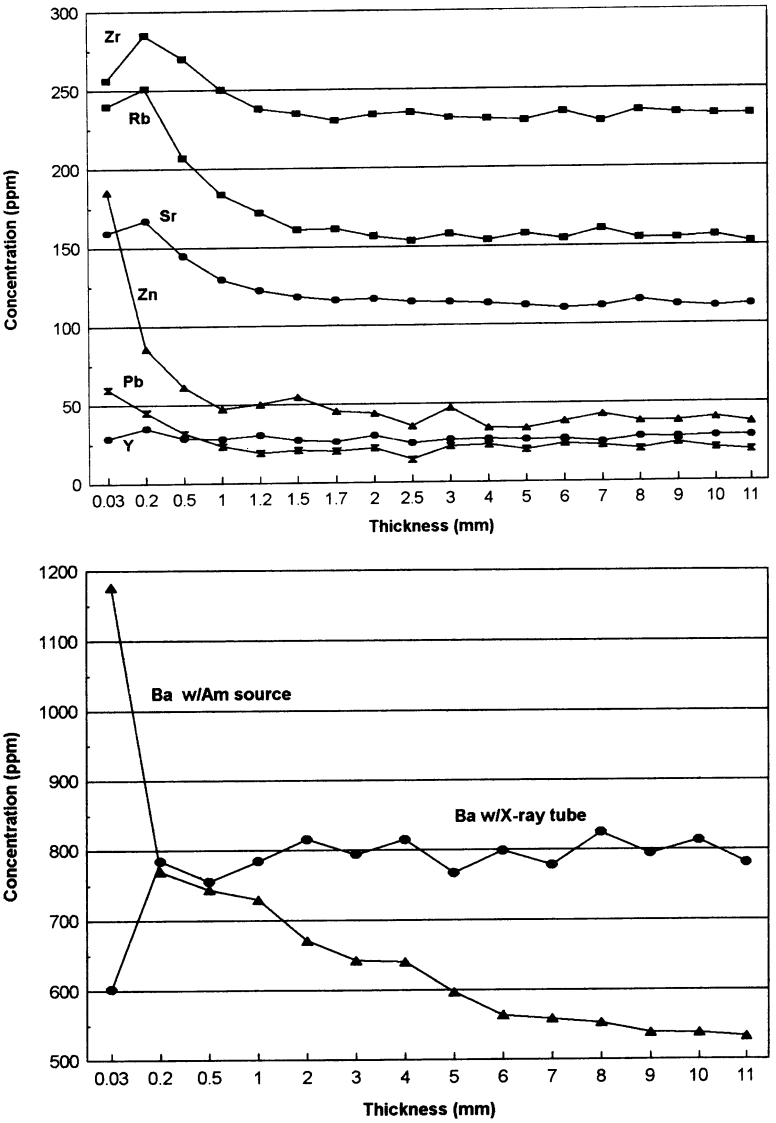


**Fig. 3.3** (**a**–**d**) Trace element values for unmodified Glass Mountain obsidian as a function of sample thickness. All concentrations reported in ppm, with the exception of Fe ($Fe_2 0_3{}^T$) which is reported in weight percent. All samples have a fixed diameter of 25 mm. (**a**) mid-*Z* elements; (**b**) Ba acquired at 50 kV with an X-ray tube, and Ba acquired with a $^{241}$Am radioisotope source; (**c**) Ti, Mn, and Fe. Ti and Mn are in ppm (left *y-axis*), and Fe is in weight percent (right *y-axis*); (**d**) Fe/Ti and Fe/Mn peak ratios

Samples were analyzed a second time for Ba using a $^{241}$Am radioisotope source on a Spectrace 440 at the XRF lab in the Department of Geology and Geophysics at the University of California, Berkeley. The system is equipped with a Si(Li) detector with a resolution of 142 eV FWHM at 5.9 keV in an area approximately 20 mm$^2$. Peak intensities for Ba were obtained by irradiating specimens with the radioisotope source for 200 s lifetime. Peak intensities were calculated as ratios to the Compton scatter peak of Am and converted to ppm by weight using linear regressions derived from the analysis of ten rock standards from the USGS, the NBS, and the GSJ.

With the exception of analysis for Ba on the Spectrace 5000 (see above), peak intensities for elements in both systems are extracted using the Super ML data analysis routine, where peak intensities for both Kα and Kβ peaks are extracted and corrected for overlap and background via comparison to stored reference standards (McCarthy and Schamber, 1981; Schamber, 1977). Analytical results for selected reference standards are given in Table 3.1 (Fig. 3.4).

## Results

### *Size Experiment*

Analytical results and sample dimensions for the Glass Mountain samples are reported in Table 3.2 and presented in Figs. 3.5 and 3.6. The accuracy of these results may be evaluated against reported element values for RGM-1, a USGS rhyolite standard also derived from the Glass Mountain obsidian flow (Tatlock et al., 1976). Trace element values for RGM-1 reported by Govindaraju (1989) are given in Table 3.1. In general, agreement between the larger Glass Mountain specimens (i.e., samples thicker than 3 mm and with a diameter of 25 mm) and RGM-1 values is quite good for most elements, though some systematic errors are evident. In the mid-*Z* analysis, element values for the elements with adequate counting statistics (i.e., Rb, Sr, and Zr) are, on average, 5% higher than the values reported for RGM-1. We suspect that this error is related to the calculation of element values for unmodified obsidian samples against calibration lines derived from the analysis of powders, due to the lower element/Compton ratio of powdered samples compared with that of unprocessed obsidian samples. Analyses of Ba with the radioisotope source are exceptionally poor. In this case, only 3 of the 26 measurements made fall within 10% of the 807 ppm reported by Govindaraju. It appears that the analyte/Compton ratio is not correcting for sample size, or that some other source of error is present.

To evaluate the precision of the results, and thus determine the point at which the trace element values are measurably affected by sample size, we compare element values of the smaller specimens to values of those samples that are well above the estimated size limits. For this purpose, we have chosen samples with a diameter of 25 mm and a minimum thickness of 4 mm as a control group. The 25 mm diameter

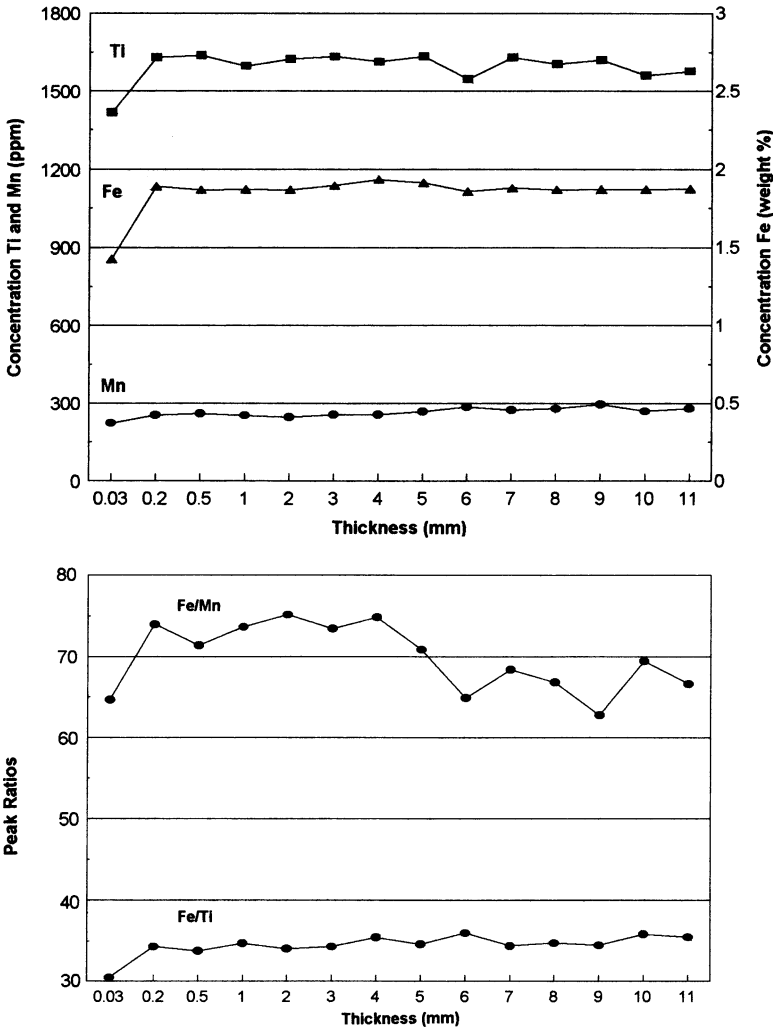


**Fig. 3.4** (**a**–**d**) Trace element values for unmodified Glass Mountain obsidian as a function of sample diameter. All concentrations reported in ppm, with the exception of Fe ($Fe_2O_3^T$) which is reported in weight percent. Samples are square with a fixed thickness of 3 mm. (**a**) mid-*Z* elements; (**b**) Ba acquired at 50 kV with an X-ray tube, and Ba acquired with a $^{241}$Am radioisotope source; (**c**) Ti, Mn, and Fe. Ti and Mn are in ppm (left *y-axis*), and Fe is in weight percent (right *y-axis*); (**d**) Fe/Ti and Fe/Mn peak ratios

samples completely cover the sample slot so that sample diameter or skewed placement of a sample should not factor into the measurements. The minimum thickness of 4 mm in the control group is well above infinite thickness for all elements except Ba, for which infinite thickness is over a centimeter at this energy. This is not ideal. However, a test of all element values in the control group revealed no systematic variation in element values relative to thickness, except for Ba

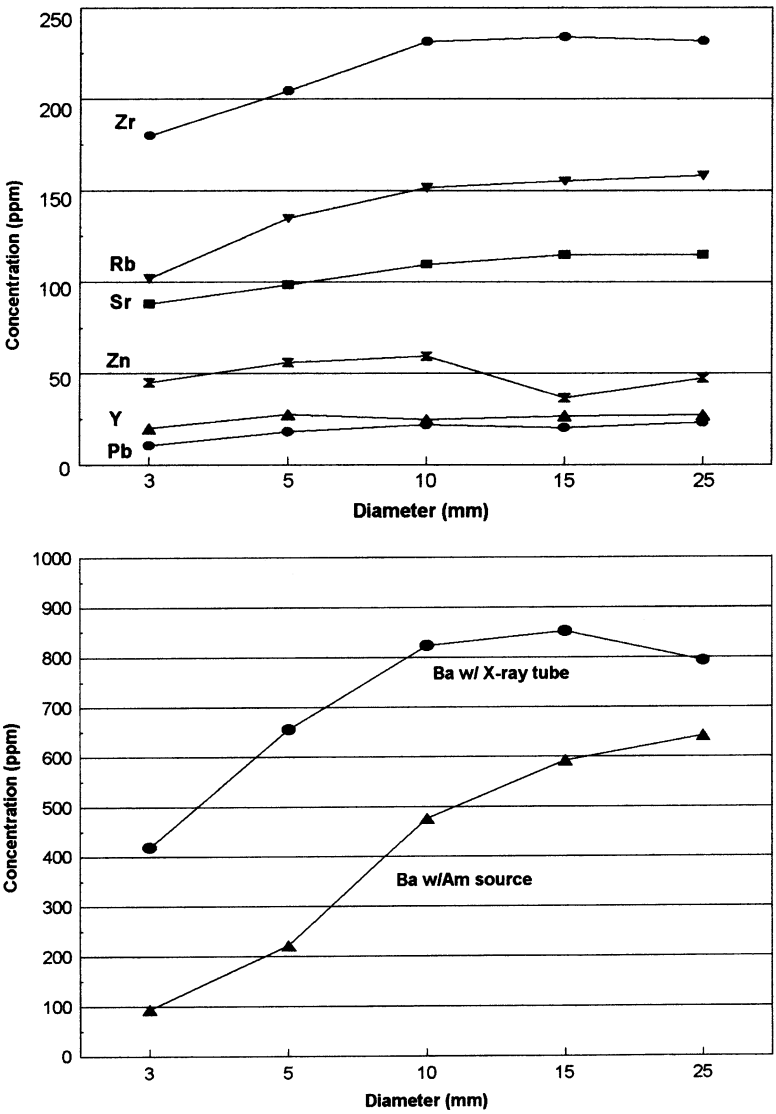


**Fig. 3.5** Relative errors acquired from six runs of Bodie Hills obsidian. Each point represents the coefficient of variance of a given element in a single sample analyzed in six different orientations. Squares represent CV for unmodified samples of obsidian with flaked surfaces (BH-1 through BH-5), while the triangle represents the CV of a pressed powder sample of Bodie Hills obsidian. Numbers in bold above each element indicate the average concentration of that element. All values are in ppm with the exception of Fe/Ti and Fe/Mn peak ratios, and Fe ($Fe_2O_3^T$) which is in weight percent. Values for Ba acquired with the $^{241}$Am radioisotope source are labeled Ba/Am

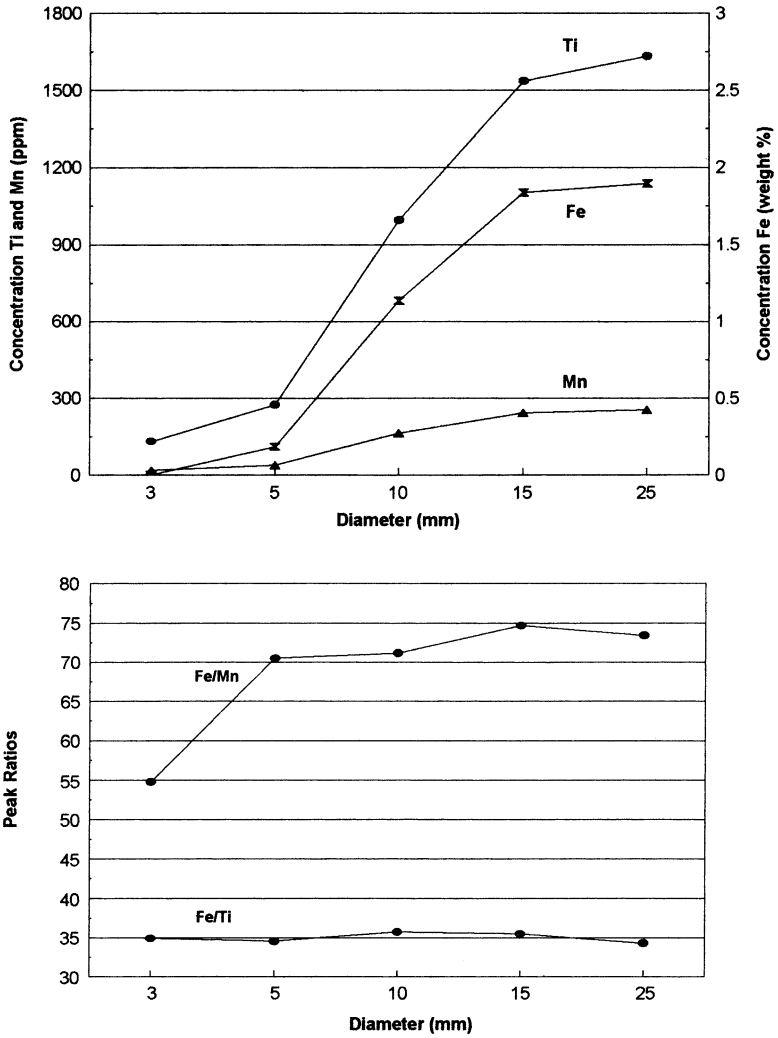


**Fig. 3.6** Relative errors acquired from six runs of Napa Valley obsidian. Each point represents the coefficient of variance of a given element in a single sample analyzed in six different orientations. Squares represent CV for unmodified samples of obsidian with flaked surfaces (NV-1 through NV-5), while the triangle represents the CV of a pressed powder sample of Napa Valley obsidian. Numbers in *bold* above each element indicate the average concentration of that element. All values are in ppm with the exception of Fe/Ti and Fe/Mn peak ratios, and Fe ($Fe_2O_3^T$) which is in weight percent. Values for Ba acquired with the $^{241}$Am radioisotope source are labeled Ba/Am

acquired with the radioisotope source. As mentioned above, precision and accuracy are poor in this analysis for all samples. For all other elements, significant deviation from the control group averages in the smaller samples should indicate the point at which sample size has affected the measurement. In Table 3.2, element values for the smaller samples appear in bold type when they differ significantly (two-sample

*t*-test at $a = 0.05$) from the control sample above. To better emphasize the general trends in the data, selected element values are depicted as a function of sample thickness in Fig. 3.5a–d and as a function of sample diameter in Fig. 3.6a.d.

At the physical level, observed element distortions are the result of two conditions – infinite thickness and the field of view of the detector. When a sample is too small to cover the area seen by the detector, the relative deficit in X-rays from the sample results in element intensities that are lower than one would expect for a given material. This effect is best illustrated in the Ti, Mn, and Fe concentration values plotted in Fig. 3.6c, where no ratio correction is employed. In this case, element values fall drastically at the 10 mm diameter.

As discussed previously, infinite thickness for a given element in an analysis depends upon sample matrix and the excitation energy used. Ultimately, however, tolerance for thickness and diameter will be determined by the way in which element values are calculated. In this study, peak ratio values (i.e., Fe/Mn and Fe/Ti) show the greatest overall success. These values are statistically indistinguishable from the control group down to a thickness of 0.2 mm for Fe/Ti and to a thickness of 0.03 mm for Fe/Mn, assuming a fixed diameter of 25 mm. The difference in precision between the two ratios (see also Figs. 3.5d and 3.6d) is likely due to the low concentration of Mn relative to that of Ti in Glass Mountain obsidian (279 ppm for Mn vs. 1,601 ppm for Ti, Govindaraju, 1989). Similarly, and at a fixed thickness of 3 mm, values are indistinguishable down to a diameter of 5 mm for Fe/Mn and 3 mm for Fe/Ti, though these limits rise to 10 mm for the 1 and 2 mm thick samples.

For analysis of Ba with the X-ray tube, ppm values are indistinguishable from the control group down to a thickness of 0.2 mm. This is an excellent result given that infinite thickness for Ba in this analysis is over 1 cm. However, the same analysis seems particularly sensitive to sample diameter. Values for two of the 15 mm diameter samples (the 2 and 3 mm thicknesses) are significantly different from the control group, though the value for the 15 mm by 1 mm thick sample is not. This points to one of the limitations of this data set, which is that too few sample diameters are analyzed to fully describe the relationship between diameter and element concentration and by extension, effects of diameter and thickness combined. For now, we assume that the allowable diameter in this analysis is somewhere between 15 and 25 mm.

Analytical results for Ba acquired with the Am source are poor for all samples. Of 27 measurements, only three (the 0.2, 0.5, and 1 mm thick samples) are within 100 ppm, or 12% of the 807 ppm reported for RGM-1 (Govindaraju, 1989). Because the analyte/Compton correction usually requires samples of infinite thickness (Franzini et al., 1976), the large infinite thickness of barium at this energy may be a factor, or perhaps some other source of error is present.

Size tolerances for elements in the mid-*Z* analysis, as defined by comparison to the control group, are somewhat diverse. In general, the results are more conclusive, and probably more reliable, for the elements with large peaks, so this discussion will focus on Rb, Sr, and Zr. Zn and Pb are seldom used in obsidian characterization, and the poor precision of these values reflects the fact that this analysis is

optimized for Rb, Sr, Y, and Zr. If required, much better results may be obtained for these elements by using a lower excitation energy. For those samples with a fixed diameter of 25 mm, element values are indistinguishable from the control group down to thicknesses of 2 mm for Rb, to 2.5 mm for Sr, and to 1.2 mm for Zr. The lower thickness limit for Zr relative to the other two elements is unexpected. As the elements are close in atomic number, they would be expected to behave similarly, relative to thickness. More likely, this difference points to inadequate sampling in the control group. In any case, substantial distortion in all three element values begins at about the 1.2 and 1 mm thicknesses (Fig. 3.5a). Results are more consistent for sample diameter. At a fixed thickness of 3 mm trace element values for all three elements are unaffected down to a diameter of 10 mm. For Sr and Zr, this threshold rises for the 2 mm thick samples, and at 1 mm thick, values for all diameters are measurably distorted.

## *Surface Experiment*

Analytical results for the surface experiment are presented in Table 3.3. By comparing the coefficients of variation (CV) for six runs of the flaked samples to six runs of powdered samples, we expected to see a difference in precision that would reflect the error contributed by the flaked surfaces. What we see instead is that for most elements, any potential difference in precision between flaked and powdered specimens is obscured by the much larger errors contributed by peak counting uncertainty. In general, the distribution of counts in an analyte peak follows the normal distribution, and a one s error is given by the square root of counts in the peak (Jenkins et al., 1981). While other factors such as peak-to-background ratio and element sensitivity contribute to the overall precision of a measurement, the effects of counting uncertainty in this analysis are apparent in Figs. 3.7 and 3.8, where the CV for the six runs on each sample are reported by element. Element concentrations, in addition to average peak counts for each element, are given in Table 3.4.

In general, and within a given spectral region, error is larger for elements where concentration and hence, peak counts are low. This is reflected in both the magnitude and range of the CV values for elements in all samples. Coefficients of variation for Mn in the Napa Valley samples, for instance, range from 1.8 to 7.8%, where Mn concentration is an average of 167 ppm, with a peak area of approximately 2,400 counts. In the Bodie Hills samples, where Mn concentration averages 487 ppm with a peak area of approximately 8,200 counts, CV ranges from 1.5 to 2.2%.

For the flaked vs. powdered sample comparison, while lower variability was expected of powdered samples, coefficients of variation (CV) for six runs of the powdered Napa Valley and Bodie Hills samples are consistently at or below the lowest CV values for the flaked samples *only* for Fe and Zr. These elements are distinguished by large peaks and high peak-to-background ratios. Only for Fe

**Table 3.3** Trace element data for 10 flaked obsidian samples (BH-1 through NV-5) and two pressed powder samples

| Sample | Zn | Pb | Rb | Sr | Y | Zr | Ti | Mn | Fe | Fe/Ti | Fe/Mn | Ba | Ba(Am) |
|---|---|---|---|---|---|---|---|---|---|---|---|---|---|
| *BH-1* | | | | | | | | | | | | | |
| Mean | 34 | 38 | 189 | 92 | 15 | 104 | 561 | 412 | 0.57 | 36 | 15 | 431 | 331 |
| Min | 27 | 35 | 186 | 90 | 12 | 101 | 529 | 403 | 0.56 | 33 | 15 | 422 | 323 |
| Max | 42 | 40 | 190 | 94 | 17 | 107 | 611 | 424 | 0.58 | 38 | 16 | 444 | 341 |
| SD | 5.2 | 2.0 | 1.3 | 1.9 | 1.8 | 2.0 | 24.8 | 6.6 | 0.01 | 1.4 | 0.3 | 8.1 | 5.8 |
| CV | 15.1 | 5.3 | 0.7 | 2.1 | 12.2 | 2.0 | 4.4 | 1.6 | 1.46 | 3.9 | 1.7 | 1.9 | 1.8 |
| *BH-2* | | | | | | | | | | | | | |
| Mean | 36 | 37 | 188 | 91 | 14 | 103 | 522 | 393 | 0.54 | 37 | 15 | 445 | 345 |
| Min | 30 | 33 | 183 | 90 | 11 | 99 | 493 | 386 | 0.50 | 35 | 15 | 433 | 341 |
| Max | 45 | 41 | 190 | 93 | 15 | 106 | 556 | 400 | 0.56 | 39 | 16 | 454 | 350 |
| SD | 4.9 | 2.8 | 2.8 | 1.1 | 1.4 | 2.7 | 23.6 | 5.1 | 0.01 | 1.4 | 0.3 | 8.6 | 3.1 |
| CV | 13.8 | 7.4 | 1.5 | 1.2 | 10.4 | 2.6 | 4.5 | 1.3 | 2.26 | 3.7 | 1.9 | 1.9 | 0.9 |
| *BH-3* | | | | | | | | | | | | | |
| Mean | 37 | 37 | 190 | 93 | 13 | 105 | 546 | 389 | 0.52 | 35 | 15 | 447 | 354 |
| Min | 28 | 36 | 186 | 91 | 12 | 101 | 538 | 377 | 0.51 | 33 | 15 | 436 | 345 |
| Max | 43 | 42 | 197 | 98 | 14 | 109 | 551 | 397 | 0.54 | 35 | 15 | 468 | 365 |
| SD | 4.5 | 2.3 | 3.6 | 2.2 | 1.0 | 2.2 | 4.2 | 8.0 | 0.01 | 0.6 | 0.2 | 10.1 | 7.3 |
| CV | 12.4 | 6.1 | 1.9 | 2.3 | 7.8 | 2.1 | 0.8 | 2.1 | 1.94 | 1.8 | 1.3 | 2.3 | 2.1 |
| *BH-4* | | | | | | | | | | | | | |
| Mean | 32 | 37 | 189 | 95 | 14 | 103 | 511 | 380 | 0.52 | 37 | 15 | 443 | 352 |
| Min | 29 | 33 | 184 | 92 | 12 | 101 | 487 | 373 | 0.51 | 36 | 15 | 436 | 345 |
| Max | 35 | 42 | 195 | 98 | 15 | 105 | 540 | 386 | 0.53 | 39 | 16 | 456 | 356 |
| SD | 2.2 | 3.1 | 3.6 | 1.9 | 0.9 | 1.3 | 18.7 | 4.9 | 0.01 | 1.2 | 0.1 | 6.5 | 4.7 |
| CV | 6.9 | 8.3 | 1.9 | 2.0 | 6.4 | 1.2 | 3.7 | 1.3 | 1.70 | 3.3 | 0.9 | 1.5 | 1.3 |
| *BH-5* | | | | | | | | | | | | | |
| Mean | 34 | 38 | 188 | 92 | 14 | 103 | 518 | 376 | 0.50 | 35 | 15 | 441 | 342 |
| Min | 29 | 36 | 179 | 91 | 12 | 97 | 502 | 364 | 0.49 | 34 | 15 | 422 | 338 |
| Max | 37 | 41 | 193 | 95 | 15 | 107 | 537 | 394 | 0.52 | 37 | 16 | 465 | 356 |
| SD | 2.9 | 1.4 | 5.1 | 1.5 | 1.1 | 3.0 | 11.4 | 10.2 | 0.01 | 0.9 | 0.5 | 13.8 | 6.6 |
| CV | 8.6 | 3.6 | 2.7 | 1.6 | 8.2 | 2.9 | 2.2 | 2.7 | 2.27 | 2.6 | 3.1 | 3.1 | 1.9 |
| *NV-1* | | | | | | | | | | | | | |
| Mean | 63 | 35 | 194 | 8 | 47 | 240 | 442 | 141 | 1.17 | 89 | 89 | 367 | 256 |
| Min | 58 | 33 | 192 | 7 | 45 | 236 | 416 | 137 | 1.15 | 82 | 88 | 354 | 251 |
| Max | 69 | 39 | 196 | 10 | 51 | 243 | 465 | 145 | 1.19 | 94 | 93 | 376 | 260 |
| SD | 4.2 | 2.0 | 1.3 | 1.0 | 2.1 | 2.3 | 15.2 | 2.4 | 0.02 | 3.8 | 2.0 | 6.7 | 3.4 |
| CV | 6.6 | 5.6 | 0.7 | 12.5 | 4.5 | 1.0 | 3.5 | 1.7 | 1.35 | 4.3 | 2.2 | 1.8 | 1.3 |
| *NV-2* | | | | | | | | | | | | | |
| Mean | 64 | 34 | 195 | 8 | 46 | 243 | 451 | 143 | 1.18 | 87 | 89 | 364 | 265 |
| Min | 58 | 32 | 193 | 6 | 40 | 239 | 433 | 129 | 1.16 | 83 | 83 | 349 | 258 |
| Max | 68 | 36 | 197 | 9 | 49 | 247 | 469 | 150 | 1.19 | 92 | 100 | 372 | 276 |
| SD | 3.5 | 1.2 | 1.5 | 1.1 | 2.8 | 2.8 | 11.6 | 7.6 | 0.01 | 2.8 | 5.9 | 8.5 | 6.2 |
| CV | 5.5 | 3.4 | 0.8 | 14.5 | 6.2 | 1.2 | 2.6 | 5.3 | 0.85 | 3.2 | 6.6 | 2.3 | 2.3 |
| *NV-3* | | | | | | | | | | | | | |
| Mean | 63 | 37 | 193 | 7 | 46 | 247 | 453 | 145 | 1.17 | 86 | 87 | 369 | 273 |
| Min | 56 | 32 | 190 | 7 | 43 | 243 | 433 | 131 | 1.14 | 82 | 84 | 362 | 256 |

(continued)

**Table 3.3** (continued)

| Sample | Zn | Pb | Rb | Sr | Y | Zr | Ti | Mn | Fe | Fe/Ti | Fe/Mn | Ba | Ba(Am) |
|---|---|---|---|---|---|---|---|---|---|---|---|---|---|
| Max | 78 | 42 | 198 | 8 | 49 | 251 | 476 | 150 | 1.19 | 90 | 97 | 381 | 287 |
| SD | 7.6 | 3.2 | 3.0 | 0.5 | 2.3 | 2.7 | 14.3 | 6.6 | 0.02 | 2.8 | 4.5 | 6.2 | 9.8 |
| CV | 12.0 | 8.9 | 1.5 | 6.5 | 5.0 | 1.1 | 3.1 | 4.6 | 1.53 | 3.2 | 5.1 | 1.7 | 3.6 |
| *NV-4* | | | | | | | | | | | | | |
| Mean | 63 | 35 | 194 | 8 | 45 | 244 | 468 | 148 | 1.19 | 84 | 87 | 367 | 268 |
| Min | 56 | 32 | 190 | 7 | 43 | 241 | 448 | 128 | 1.17 | 81 | 80 | 359 | 264 |
| Max | 65 | 38 | 198 | 10 | 47 | 250 | 485 | 159 | 1.23 | 87 | 100 | 372 | 273 |
| SD | 3.2 | 2.1 | 2.6 | 0.8 | 1.2 | 3.1 | 12.9 | 11.0 | 0.02 | 2.2 | 7.9 | 5.4 | 2.8 |
| CV | 5.0 | 6.1 | 1.3 | 9.5 | 2.7 | 1.3 | 2.8 | 7.5 | 1.64 | 2.6 | 9.1 | 1.5 | 1.0 |
| *NV-5* | | | | | | | | | | | | | |
| Mean | 63 | 35 | 194 | 8 | 46 | 239 | 451 | 145 | 1.19 | 88 | 88 | 365 | 265 |
| Min | 56 | 33 | 191 | 5 | 45 | 236 | 416 | 133 | 1.17 | 83 | 80 | 348 | 257 |
| Max | 68 | 38 | 199 | 10 | 47 | 242 | 472 | 157 | 1.26 | 96 | 96 | 380 | 272 |
| SD | 3.4 | 1.8 | 2.8 | 1.4 | 0.7 | 1.9 | 18.6 | 8.1 | 0.03 | 3.9 | 5.2 | 11.0 | 5.2 |
| CV | 5.5 | 5.1 | 1.4 | 18.2 | 1.6 | 0.8 | 4.1 | 5.6 | 2.54 | 4.4 | 5.9 | 3.0 | 2.0 |
| *NV powder* | | | | | | | | | | | | | |
| Mean | 59 | 34 | 189 | 8 | 45 | 240 | 526 | 167 | 1.42 | 88 | 89 | 385 | 375 |
| Min | 54 | 30 | 184 | 6 | 42 | 237 | 496 | 155 | 1.41 | 83 | 86 | 373 | 332 |
| Max | 68 | 38 | 194 | 9 | 48 | 243 | 556 | 172 | 1.43 | 93 | 96 | 394 | 418 |
| SD | 4.9 | 2.7 | 3.3 | 1.0 | 2.3 | 2.1 | 20.2 | 6.5 | 0.01 | 3.6 | 3.8 | 6.2 | 39.1 |
| CV | 8.3 | 8.0 | 1.7 | 13.2 | 5.0 | 0.9 | 3.8 | 3.9 | 0.39 | 4.1 | 4.2 | 1.6 | 10.5 |
| *BH powder* | | | | | | | | | | | | | |
| X | 32 | 34 | 180 | 89 | 14 | 107 | 638 | 487 | 0.72 | 38 | 16 | 463 | 374 |
| Min | 26 | 31 | 177 | 87 | 13 | 105 | 598 | 479 | 0.72 | 35 | 15 | 446 | 342 |
| Max | 43 | 36 | 182 | 92 | 15 | 109 | 688 | 500 | 0.73 | 41 | 16 | 483 | 403 |
| SD | 5.2 | 1.7 | 1.6 | 1.5 | 0.7 | 1.2 | 27.9 | 6.6 | 0.00 | 1.9 | 0.2 | 11.9 | 27.2 |
| CV | 16.4 | 4.9 | 0.9 | 1.7 | 5.1 | 1.2 | 4.4 | 1.4 | 0.41 | 4.9 | 1.6 | 2.6 | 7.3 |
| *RGM-1 standard* | | | | | | | | | | | | | |
| X | 37 | 22 | 151 | 103 | 25 | 221 | 1665 | 291 | 2.01 | 36 | 69 | 803 | 791 |
| Min | 31 | 20 | 149 | 101 | 22 | 218 | 1638 | 285 | 2.00 | 35 | 67 | 794 | 739 |
| Max | 44 | 25 | 154 | 107 | 26 | 224 | 1687 | 297 | 2.02 | 37 | 70 | 819 | 824 |
| SD | 3.9 | 1.7 | 1.4 | 1.8 | 1.2 | 2.1 | 15.0 | 4.2 | 0.01 | 0.5 | 1.1 | 9.0 | 26.8 |
| CV | 10.5 | 7.7 | 1.0 | 1.7 | 4.8 | 0.9 | 0.9 | 1.4 | 0.39 | 1.3 | 1.7 | 1.1 | 3.4 |
| *JR-2 standard* | | | | | | | | | | | | | |
| X | 38 | 22 | 150 | 102 | 25 | 219 | 403 | 1000 | 0.80 | 70 | 8 | – | – |
| Min | 34 | 20 | 145 | 100 | 23 | 218 | 393 | 992 | 0.80 | 67 | 8 | – | – |
| Max | 42 | 24 | 152 | 103 | 28 | 221 | 415 | 1007 | 0.81 | 72 | 8 | – | – |
| SD | 3.0 | 1.4 | 2.5 | 1.3 | 1.5 | 1.4 | 7.4 | 4.6 | 0.00 | 1.5 | 0.1 | – | – |
| CV | 7.9 | 6.2 | 1.7 | 1.3 | 5.8 | 0.6 | 1.8 | 0.5 | 0.28 | 2.2 | 0.7 | – | – |

RGM-1 and JR-2 reference standards are also included. Statistics for all samples represent six runs in six different orientations. All element values are expressed in ppm with the exception of Fe/Mn and Fe/Ti peak ratios, and Fe ($Fe_2O_3^T$), which is expressed in weight percent. Values for Ba acquired with the $^{241}$Am radioisotope source are labeled Ba(Am)

are the CV of the powdered sample actually *lower* than the CV of the flaked samples. Furthermore, the difference between the two is quite small – a difference of 1.05 units of CV for the Bodie Hills samples and 0.46 units of CV for the Napa Valley samples (Figs. 3.7 and 3.8, Table 3.3). These data suggest that in most cases errors related to

**Table 3.4** Concentration values and approximate peak counts for powdered Napa Valley and Bodie Hills samples

| Element | Napa Valley | | Bodie Hills | |
|---|---|---|---|---|
| | Concentration | Counts | Concentration | Counts |
| Zn | 59 | 750 | 32 | 350 |
| Pb | 34 | 800 | 34 | 900 |
| Rb | 189 | 17,800 | 180 | 17,200 |
| Sr | 8 | 700 | 89 | 700 |
| Y | 45 | 6,600 | 14 | 1,700 |
| Zr | 240 | 40,600 | 107 | 16,500 |
| Ti | 526 | 2,800 | 638 | 3,400 |
| Mn | 167 | 2,400 | 487 | 8,200 |
| Fe | 1.41 | 238,000 | 1 | 130,000 |
| Ba | 384 | 32,000 | 463 | 36,000 |
| Ba(Am) | 341 | 4,600 | 407 | 7,200 |

All concentrations are in ppm, with the exception of Fe ($Fe_2O_3^T$), which is in weight percent. Values for barium acquired with the $^{241}$Am radioisotope source are labeled Ba(Am)

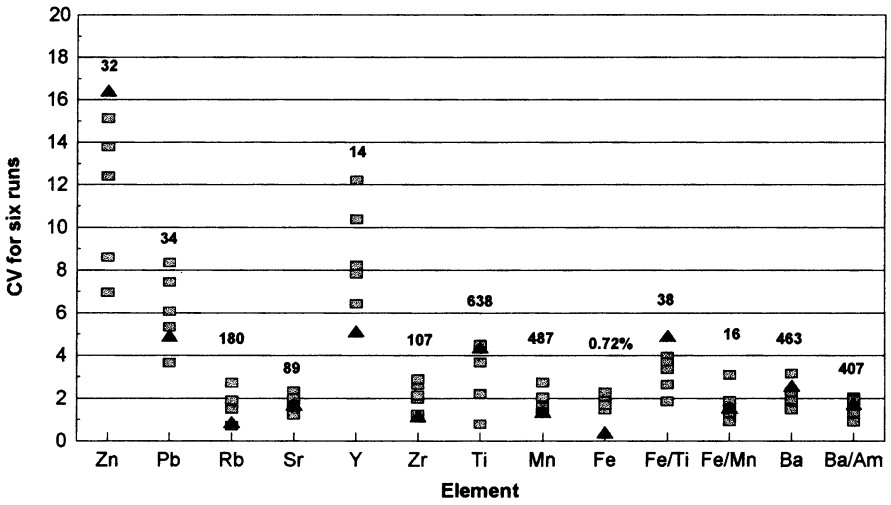


**Fig. 3.7** Relative errors acquired from six runs of Bodie Hills obsidian. Each point represents the coefficient of variance (CV) of a given element in a single sample analyzed in six different orientations. Squares represent CV for unmodified samples of obsidian with flaked surfaces (BH-1 through BH-5), while the triangle represents the CV of a pressed powder sample of Bodie Hills obsidian. Numbers in bold above each element indicate the average concentration of that element. All values in ppm with the exception of Fe/Ti and Fe/Mn peak ratios, and Fe ($Fe_2O_3^T$) which is in weight percent. Values for Ba acquired with the $^{241}$Am radioisotope source are labeled Ba/Am.

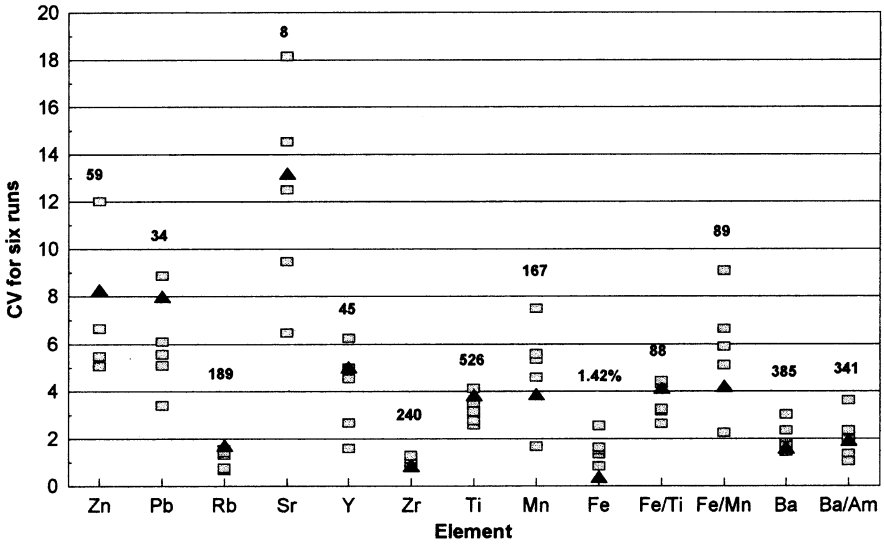


**Fig. 3.8** Relative errors acquired from six runs of Napa Valley obsidian. Each point represents the coefficient of variance (CV) of a given element in a single sample analyzed in six different orientations. Squares represent CV for unmodified samples of obsidian with flaked surfaces (NV-1 through NV-5), while the triangle represents the CV of a pressed powder sample of Bodie Hills obsidian. Numbers in bold above each element indicate the average concentration of that element. All values in ppm with the exception of Fe/Ti and Fe/Mn peak ratios, and Fe ($Fe_2O_3^T$) which is in weight percent. Values for Ba acquired with the $^{241}$Am radioisotope source are labeled Ba/Am

the surface topography of obsidian artifacts are negligible when compared to those contributed by counting uncertainty.

## Conclusions

Two experiments were conducted to measure effects related to artifact size and surface variability in the non-destructive analysis of obsidian. On the basis of the analysis of 20 samples of Glass Mountain obsidian, the following size limits are observed. Thickness limits assume a fixed sample diameter of 25 mm, and diameter limits assume a fixed thickness of 3 mm. For Fe/Mn and Fe/Ti peak ratios element values are unaffected down to a thickness of 0.2 mm and to a diameter of 5 mm. Similarly, limits for Ba acquired with the X-ray tube are 0.2 mm for thickness and somewhere between 15 and 25 mm for diameter. Results for Ba acquired with the Am radioisotope source are poor for all samples, and we are unable to explain the source of error at this time. For the mid-Z elements, the observed thickness limit ranges between 1.2 and 2.5 mm, and the diameter limit is 10 mm.

Archaeologists requiring the analysis of small artifacts will want to note that the size limits reported here reflect the points to which no statistically measurable element distortions are observed. Such a level of precision is rarely required for accurate source ascription of obsidian artifacts, and element values for many of the smaller samples in this set reflect only minor error. Furthermore, relative element proportions often remain intact, even for significantly undersized samples (e.g., 0.5 mm thick by 8 mm in diameter), and may be accurately characterized in some cases depending upon the context of the analysis. It is up to the archaeologist and the analyst to determine the analytical precision required to distinguish sources or chemical groups in a given study area.

Results of the surface experiment, where samples of flaked Napa Valley and Bodie Hills obsidian were analyzed in an attempt to measure error related to surface irregularities, suggest that this error is nearly always negligible when compared to counting uncertainty. The only instance where precision for powdered samples (CV over six runs of one sample) differs visibly from those of flaked samples is for the element Fe, where the peak is large and peak-to-background ratio is high (Figs. 3.7 and 3.8, Table 3.3). In this case, precision for the powdered samples improved over those of the flaked samples by an average of less than 1% CV for both the Bodie Hills and Napa Valley samples.

Regarding the applicability of these results to the analysis of artifacts, all samples in this study were prepared from freshly broken and clean obsidian, which is, needless to say, uncommon in the world of obsidian artifacts. Effects due to soil contamination and weathering are not considered here. Secondly, the flaked samples used in the surface experiment are relatively flat so that the convexity often encountered in flaked stone tools is not represented. Finally, these results are specific to the analytical conditions outlined herein and may or may not be comparable to results from other laboratories. For this reason, it is important that analytical methods and conditions be reported completely with the XRF results so that comparability may be evaluated.

## References

Bouey, P., (1991), Recognizing the limits of archaeological applications of non-destructive energy-dispersive X-ray fluorescence analysis of obsidians. *Materials Research Society Proceedings* 185, 309–320.

Davis, M.K., (1994), Bremsstrahlung ratio technique applied to the non-destructive energy-dispersive X-ray fluorescence analysis of obsidian. *International Association for Obsidian Studies Bulletin* 11.

Franzini, M., Leoni, L., and Saitta M., (1976), Determination of the X-ray fluorescence mass absorption coefficient by measurement of the intensity of Ag Kα Compton scattered radiation. *X-ray Spectrometry* 5:84–87.

Govindaraju, K., (1989), 1989 Compilation of working values and sample description for 272 geostandards. *Geostandards Newsletter* 13 (special issue).

Jenkins, R., Gould, R.W., and Gedcke, D., (1981), *Quantitative X-ray Spectrometry*. New York: Marcel Dekker

Hughes, R.E., (1984), Obsidian source studies in the Great Basin: Problems and Prospects. In Hughes, R.E., Ed., *Obsidian Studies in the Great Basin*, (pp. 1–20). Berkeley: Contributions of the University of California Archaeological Research Facility 45.

Hughes RE (1988), The Coso Volcanic field reexamined: implications for obsidian sourcing and hydration dating research. Geoarchaeology 3:253–265

Jackson, T.L. and Hampel, J.H., (1992), Size effects in the energy-dispersive X-ray fluorescence (EDXRF) analysis of archaeological obsidian artifacts. Presented at the 28th International Symposium on Archaeometry, Los Angeles.

McCarthy, J.J. and Schamber, F.H., (1981), Least-squares fit with digital filter: a status report. In Heinrich, K.F.J., Newbury, D.E., Myklebust, R.L. and Fiori, E. Eds., *Energy Dispersive X-ray Spectrometry*, (pp. 273–296). Washington, D.C.: National Bureau of Standards Special Publication 604.

Schamber, F.H., (1977), A modification of the linear least-squares fitting method which provides continuum suppression. In Dzubay, T.G., Ed., *X-ray Fluorescence Analysis of Environmental Samples*, (pp. 241–257). Ann Arbor: Ann Arbor Science.

Shackley MS (1988), Sources of archaeological obsidian in the Southwest: an archaeological, petrological, and geochemical study. American Antiquity 53:752–772

Shackley,M.S. and Hampel, J., (1992), Surface effects in the energy dispersive X-ray fluorescence (EDXRF) analysis of archaeological obsidian. Presented at the 28th International Symposium on Archaeometry, Los Angeles.

Tatlock, D.B., Flanagan, F.J., Bastron, H., Berman, S., and Sutton, A.L. Jr., (1976), Rhyolite, RGM-1, from Glass Mountain, California. In Flanagan, F.J., Ed., *Descriptions and Analyses of Eight New USGS Rock Standards*. U.S. Geological Survey Professional Paper 850, (pp. 11–14).